Supplement of Atmos. Chem. Phys., 25, 1949–1963, 2025
https://doi.org/10.5194/acp-25-1949-2025-supplement

Atmospheric Chemistry and Physics
Open Access

Supplement of

Air-pollution-satellite-based CO_2 emission inversion: system evaluation, sensitivity analysis, and future research direction

Hui Li et al.

Correspondence to: Bo Zheng (bozheng@sz.tsinghua.edu.cn)

Section S1. Bottom-up estimates

To derive a sector-specific prior, we update the 2019 Multi-resolution Emission Inventory for China (MEIC) (Zheng et al., 2018) using a range of activity data. The bottom-up estimation follows two primary steps: first, we apply monthly updates based on year-on-year national activity ratios obtained from the National Bureau of Statistics (https://data.stats.gov.cn/english/easyquery.htm?cn=C01); second, we disaggregate monthly emissions into daily estimates using multi-source data. The specific data sources used in this bottom-up approach are detailed in Table S1.

For emission factors (EFs), we assume a yearly halving of the reduction rate in NO_x EFs. Since 2012, NO_x emissions have sharply decreased due to effective pollution control measures with many end-of-pipe devices; however, the rate of decline has slowed in recent years, reflecting the diminishing potential for further reductions (Geng et al., 2024; Li et al., 2023). As such, the default assumption is that the reduction rate in NO_x EFs halves each year, consistent with the limited potential for continued reductions. By contrast, CO_2 EFs are assumed to remain constant over time, as they are primarily influenced by fuel type and combustion conditions (Cheng et al., 2021).

Section S2. CO_2-to-NO_x emission ratios

In this inversion system, the CO_2-to-NO_x emission ratios (ERs) are initially derived from the 2019 MEIC inventory, then updated for the target year (2022 in this study) by assuming a specific reduction in NO_x EFs by sector while keeping CO_2 EFs constant. This approach aligns with the ongoing decline in NO_x emissions due to pollution control measures, while CO_2 emissions remain more closely tied to fuel type and combustion conditions (Text S1). Accordingly, the CO_2-to-NO_x ERs are dependent on the reduction ratio of NO_x EFs in this system (represented by the $rNO_{x\,s,i,y}$ in Eq. 5).

The reduction ratio of NO_x EFs first influences the disaggregation of total NO_x emissions to sectors, and then affects the sector-specific conversion from NO_x to CO_2 emissions. To evaluate this impact, we set a gradient test with a NO_x EFs reduction range from 1% to 10% (ef_[-10%, -1%]). Results indicate a notable impact on CO_2 emissions, affecting annual national CO_2 totals by up to 10.7% (Details discussed in Manuscript). This finding emphasizes the need for a more precise approach to setting NO_x emission reduction ratios in future refinements, such as incorporating an iterative adjustment within the bottom-up process to better align bottom-up and TROPOMI-constrained sectoral NO_x emissions (as mentioned in the Discussion).

We further compare the CO_2-to-NO_x ERs of MEIC with some international inventories, including the Emissions Database for Global Atmospheric Research (EDGAR, https://edgar.jrc.ec.europa.eu/dataset_ap81) (Crippa et al., 2020) and the Community Emissions Data System (CEDS) (Mcduffie et al., 2020), for the year 2019. Given the different categorization structures in these inventories, we focus on comparing the overall CO_2-to-NO_x ERs, which are 493.7 for MEIC, 571.5 for EDGAR, and 462.6 for CEDS. The emission factors in MEIC are more spatially and sectorally refined for China, making its CO_2-to-NO_x ERs more representative of China-specific emissions (Zheng et al., 2018).

Section S3. Tests affecting NO_x and CO_2 emissions result in similar impacts

Among tests, Res_2×2.5 and 2021_base are the most influential ones, triggering $\overline{RC_t} \pm 1\sigma_t$ of -2.8%±6.2% (-1.2%±6.0%) and 0.5%±8.6% (-0.6%±6.9%) in daily national total NO_x (CO_2) emissions, respectively. Trop_fill and Trop_v2.3 come next, causing variations of 1.1%±5.3% (1.3%±3.9%) and -0.5%±6.7% (-0.4%±5.9%) in daily national total NO_x (CO_2) emissions. In contrast, β_[-20%, 20%] leads to notable but consistent variations in NO_x and CO_2, linearly strengthening its impact as the adjustment amplitude increases, wherein β_-20% triggers 3.0%±3.2% in NO_x emissions and 2.6%±3.0% in CO_2 emissions (Fig. S7).

Section S4. Response of sectoral NO_x emissions to tests

The residential sector is the most vulnerable to 2021_base, with variations up to -6.0%±6.7% in daily NO_x emissions. Residential emissions exclusively present sensitivity to 4_sectors, thre_04, and thre_06, with variations of -6.1%±2.5%, 7.4%±7.8%, and -6.4%±5.6% in its NO_x emissions, respectively. The industry and transport emissions are more sensitive to the β_[-20%, 20%], with $\overline{RC_s} \pm 1\sigma_s$ up to 4.1%±4.5% and 4.5%±6.1% in NO_x emissions under β_-20%. Res_2×2.5 incurs the $\overline{RC_s} \pm 1\sigma_s$ of -8.3%±12.4% and -2.7%±8.8% in daily national NO_x emissions in transport and power sectors, respectively.

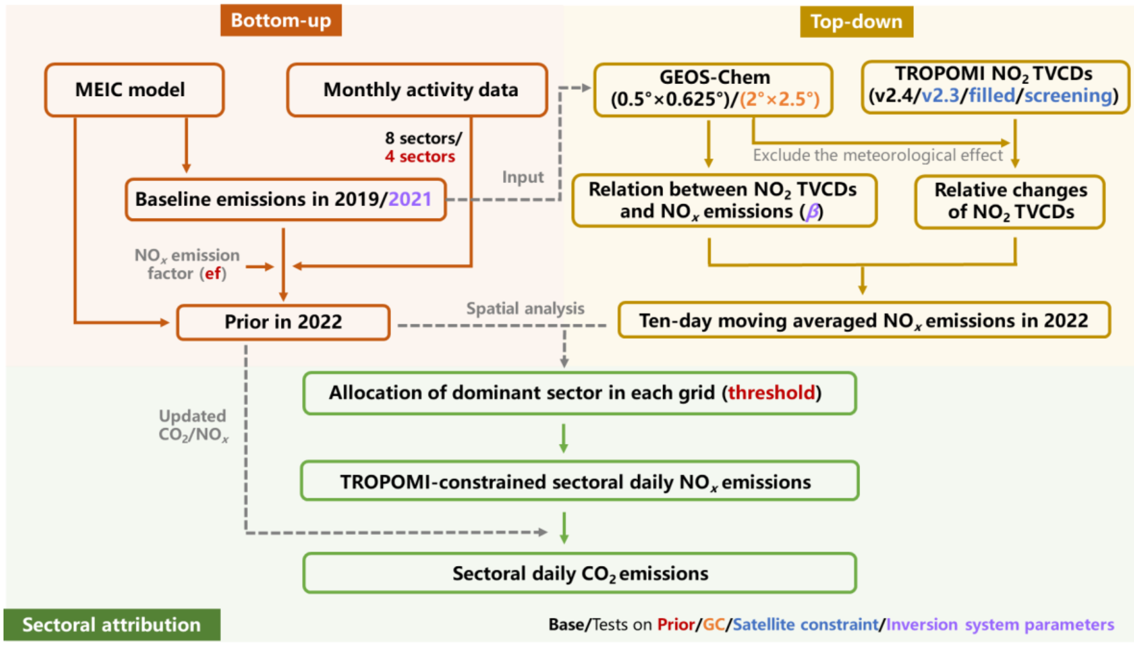

Figure S1. **The methodology of the inversion system and the tests we introduced.** Sensitivity tests include prior (red labeled), model resolution (orange labeled), satellite data (blue labeled), and inversion system parameters (purple labeled). Detailed settings are seen in Tables 1 and 2.

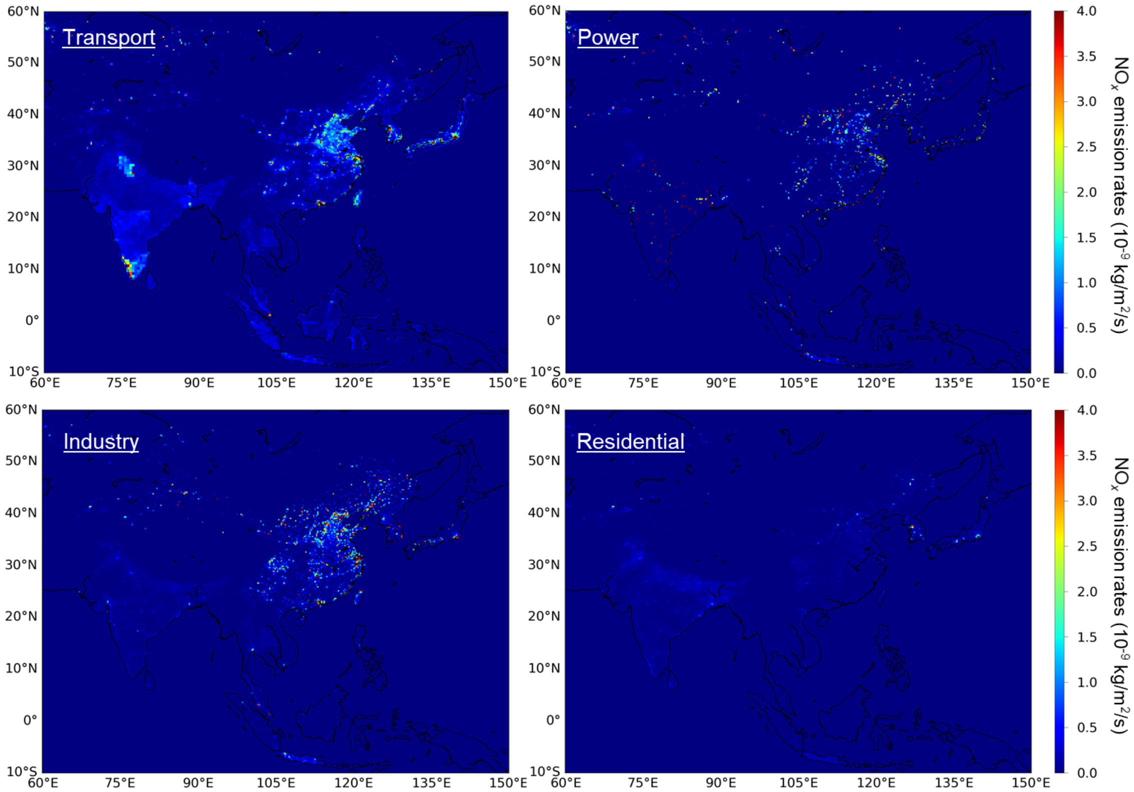

Figure S2. Sectoral NO_x emissions in 2019 used in this study (0.25°×0.25°). MEIC inventory is used within China.

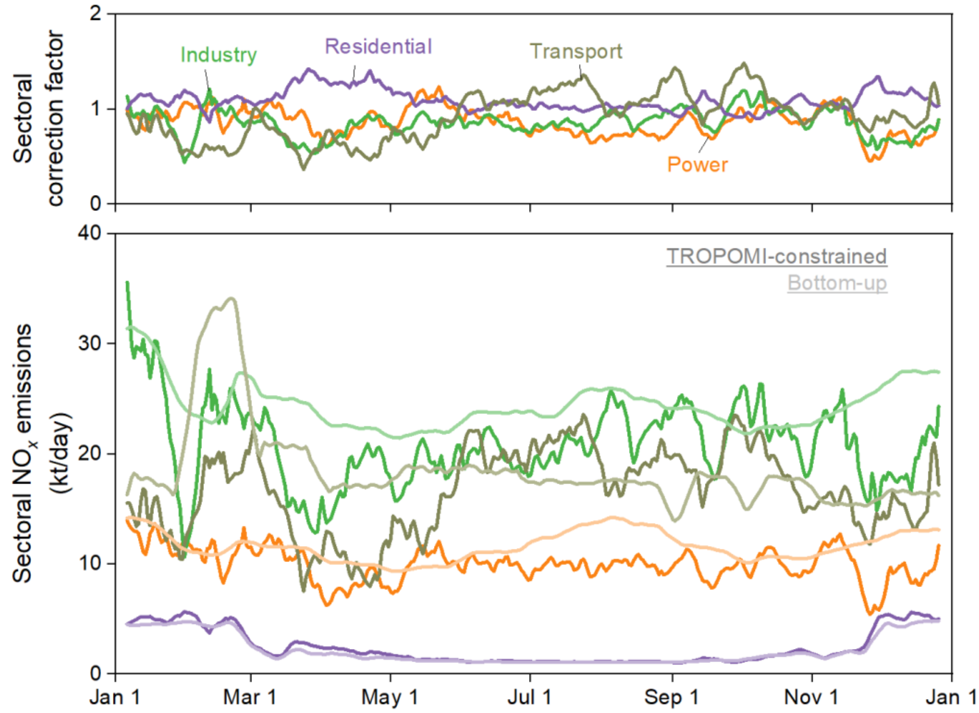

Figure S3. **The comparison between bottom-up and TROPOMI-constrained sectoral emissions (base inversion).** The upper panel shows the sectoral correction factors.

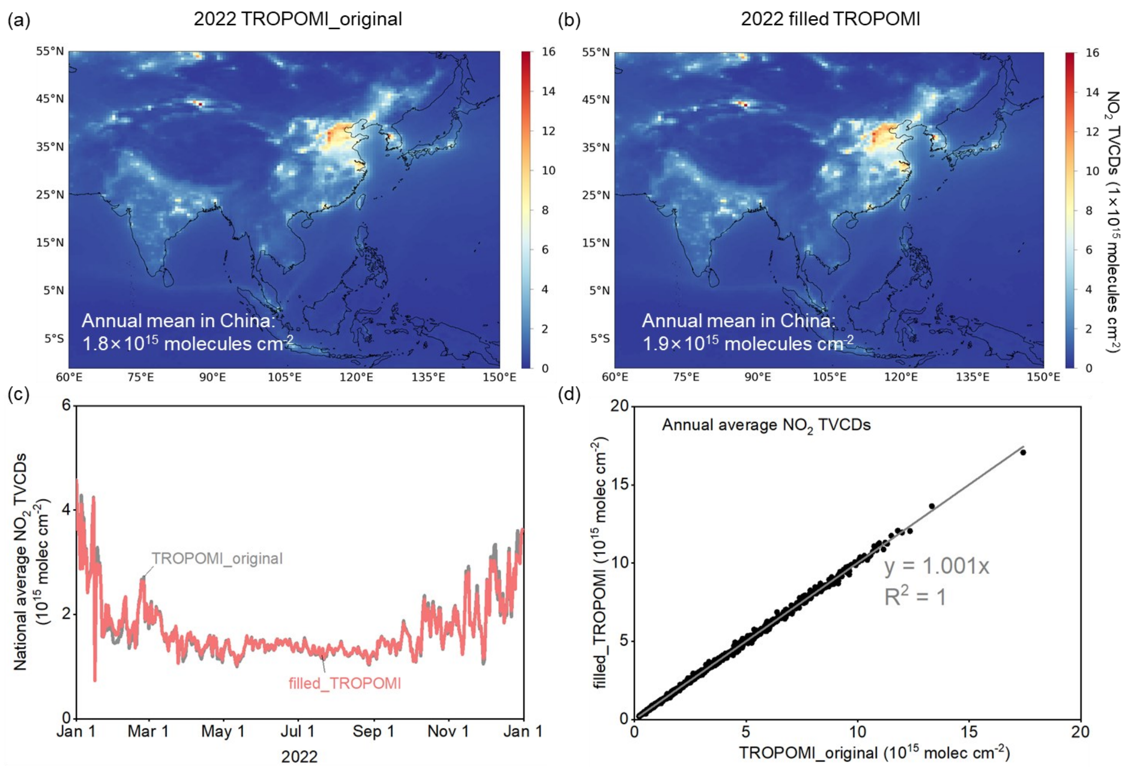

Figure S4. **The comparison of XGBoost filled TROPOMI and original TROPOMI NO_2 TVCDs in 2022 in China.** (**a**) shows the annual mean NO_2 TVCDs of original TROPOMI sampling. (**b**) shows the annual mean NO_2 TVCDs of filled TROPOMI using XGBoost method. (**c**) compares the daily national mean NO_2 TVCDs between original and filled TROPOMI. (**d**) shows the correlation between original and filled TROPOMI NO_2 TVCDs grid-by-grid. Note that regions outside China in (a) and (b) are plotted with the original TROPOMI data in 2022, while the data in (c) and (d) are exclusively for China.

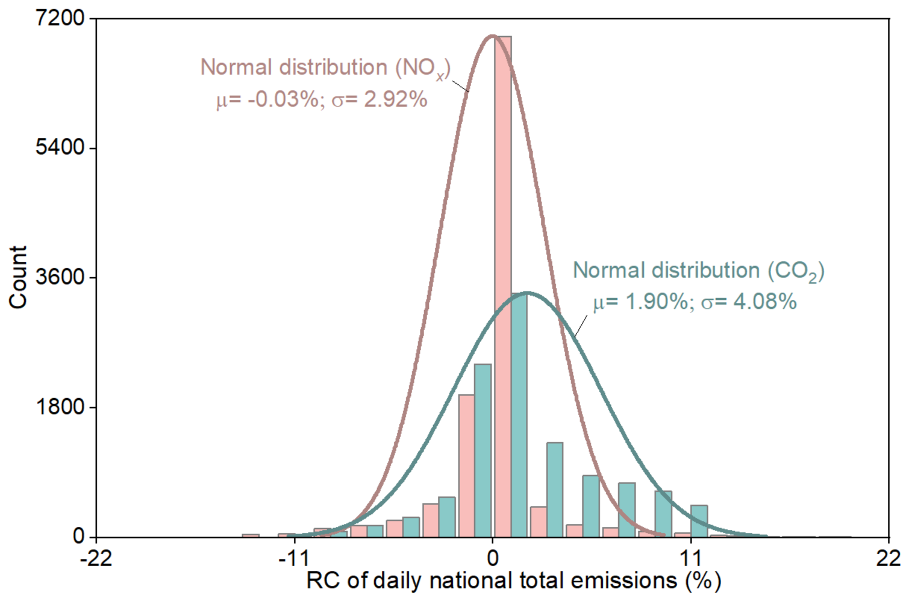

Figure S5. **RC distribution of daily national total emissions under all tests.** The overall distribution of RC of daily national total emissions of NO_x and CO_2 across all tests adheres to a normal distribution. For NO_x, the mean (μ) and standard deviation (σ) are -0.03% and 2.92%, respectively, while for CO_2, they are 1.90% and 4.08%. Given our discussion focusing on CO_2 emissions, 1σ = 4.0% is thus chosen as the threshold for distinguishing between consistent and inconsistent impacts.

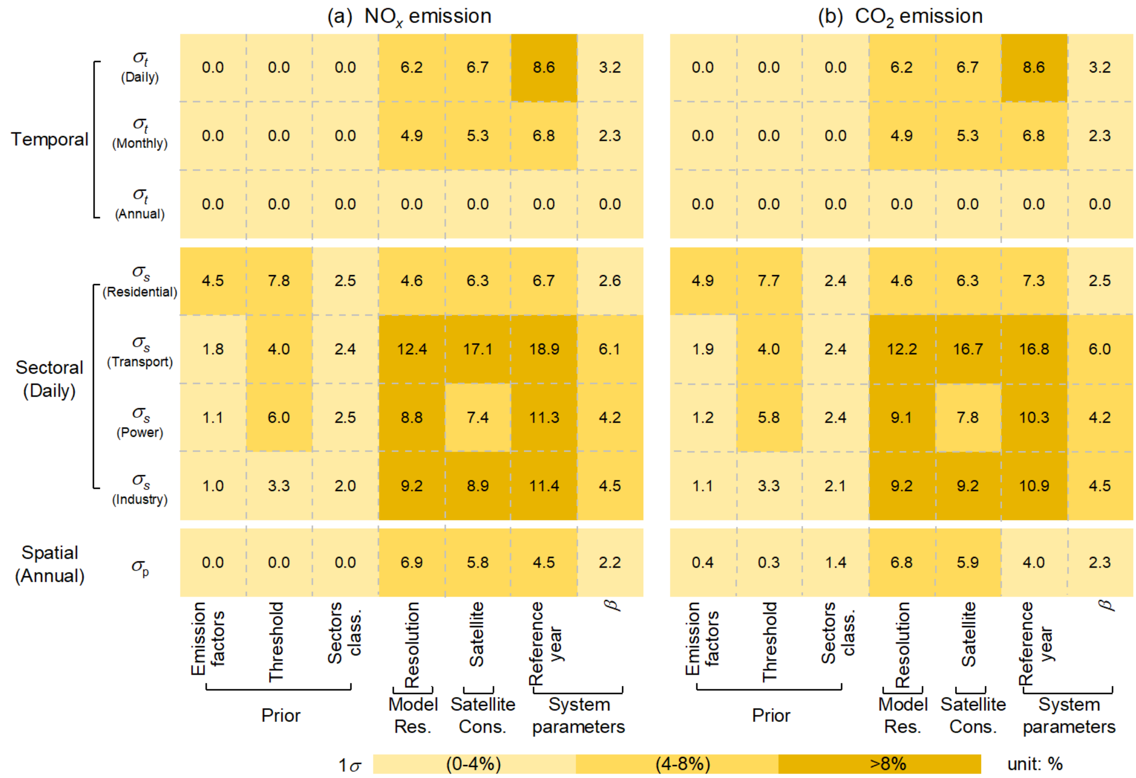

Figure S6. An overview of consistency of tests' impacts on (a) NO_x and (b) CO_2 emissions across finer scales. The orange color signifies one standard deviation (1σ), reflecting the degree of consistency in the impact of the corresponding test. A larger 1σ indicates greater inconsistency. Sectoral emissions consistency is depicted on a daily scale, and spatial results are depicted on an annual provincial scale. The numbers within each grid represent the corresponding 1σ on a certain dimension under tests.

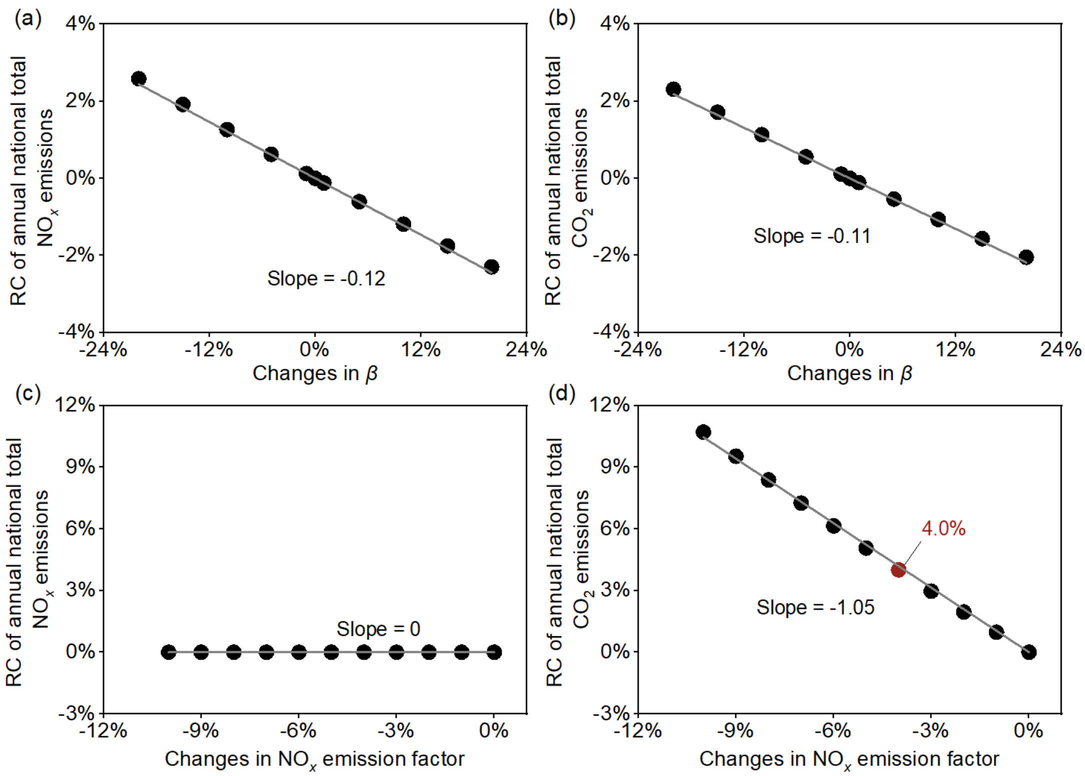

Figure S7. Sensitivity of annual national total NO_x and CO_2 emissions to β and NO_x emission factor. (**a**) and (**c**) present the estimated NO_x emissions under a ten-level gradient for β and emission factor variations. (**b**) and (**d**) are plotted for CO_2 emissions as (**a**) and (**c**).

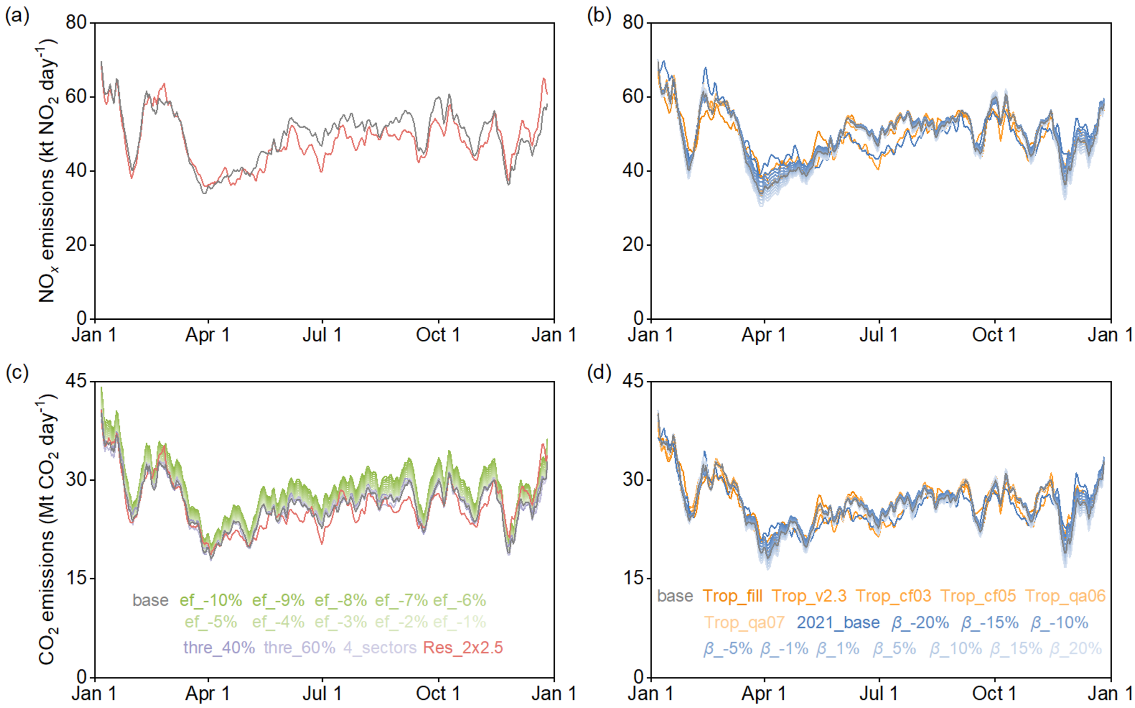

Figure S8. **Ten-day moving average NO_x and CO_2 emissions in 2022 under different sensitivity tests.** (**a**) and (**b**) present the ten-day moving NO_x emissions under all tests and base. (**c**) and (**d**) are plotted for CO_2 emissions as (**a**) and (**b**).

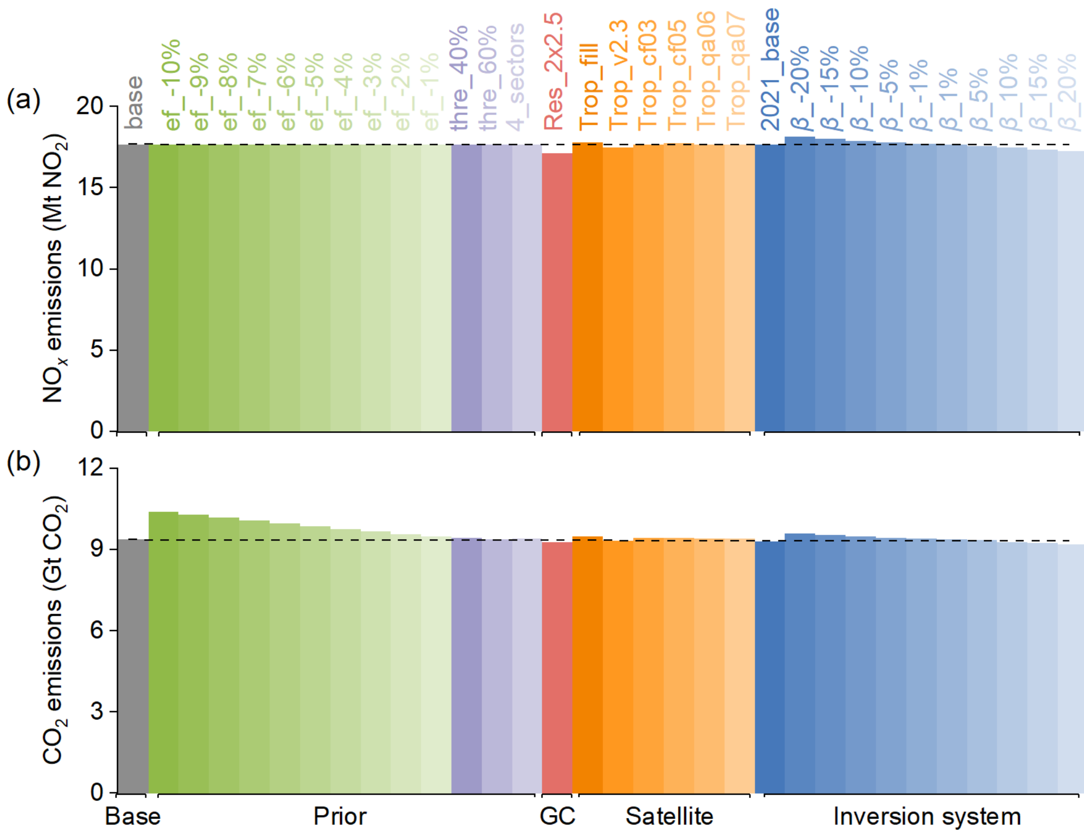

Figure S9. **Comparison of total (a) NO_x and (b) CO_2 emissions in 2022 under various sensitivity tests.** Label above each column refer to the corresponding tests.

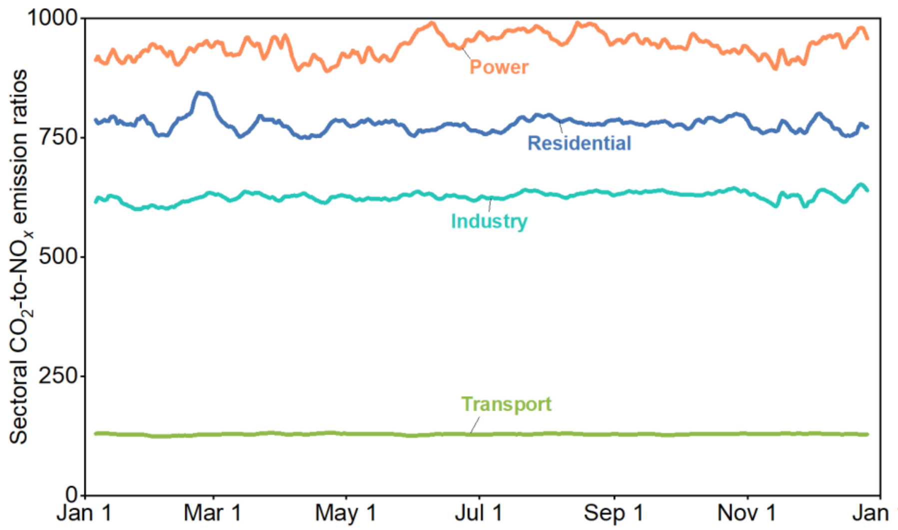

Figure S10. **Sectoral CO_2-to-NO_x emission ratios in 2022 under base inversion.** Sectors are color-coded.

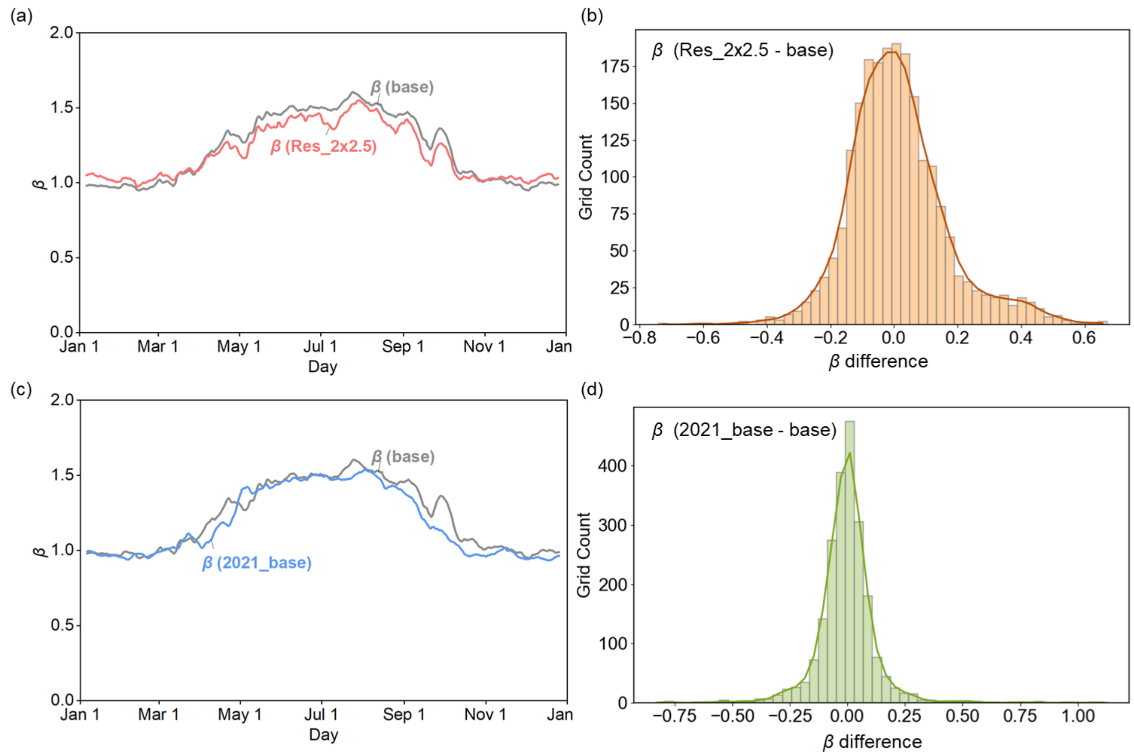

Figure S11. **Comparison of *β* between Res_2×2.5 and base, 2021_base and base.** (**a**) and (**c**) compare the daily *β* dynamics between Res_2×2.5 and base, and between 2021_base and base, respectively. (**b**) and (**d**) present the grid distribution of *β* variance between Res_2×2.5 and base, and between 2021_base and base, respectively.

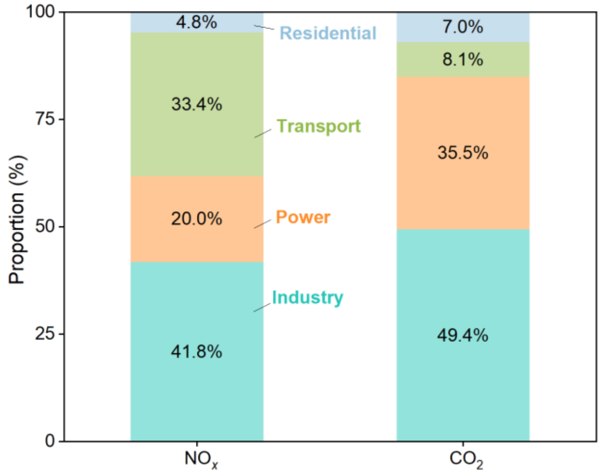

Figure S12. Sectoral contribution to total NO_x and CO_2 emissions in 2022 under base inversion. Sectors are color-coded.

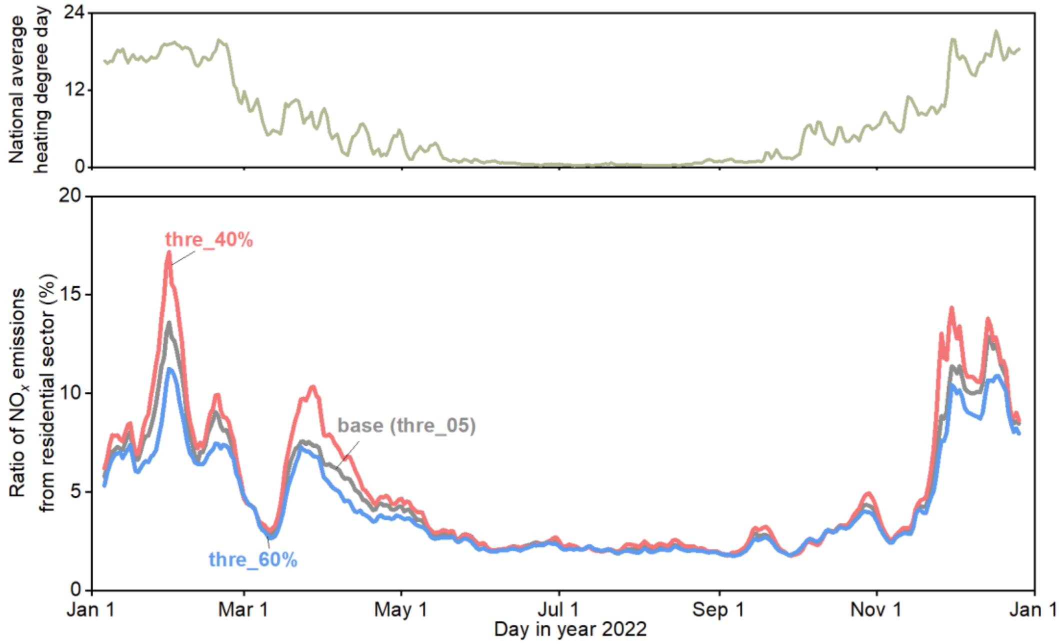

Figure S13. **The comparison of proportion attributing total TROPOMI-constrained NO_x emissions to the residential sector.** Black, red, and blue lines refer to the base, thre_40%, and thre_60% inversions, respectively. The upper panel displays the temporal variation of the national average heating degree day.

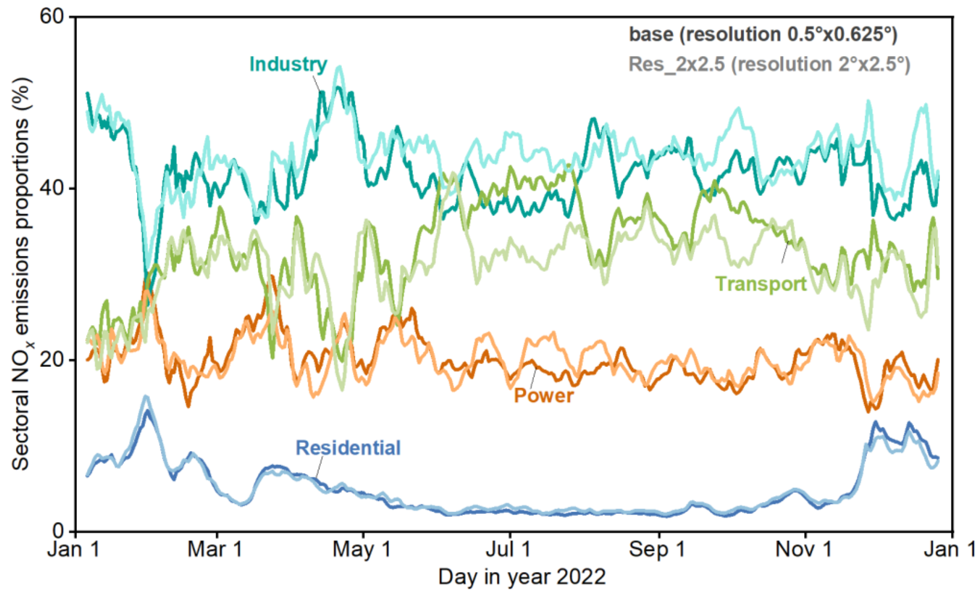

Figure S14. **The comparison of the sectoral proportion of TROPOMI-constrained NO_x emissions.** Sectors are color-coded. Deep color refers to the base inversion, and light color represents the Res_2×2.5.

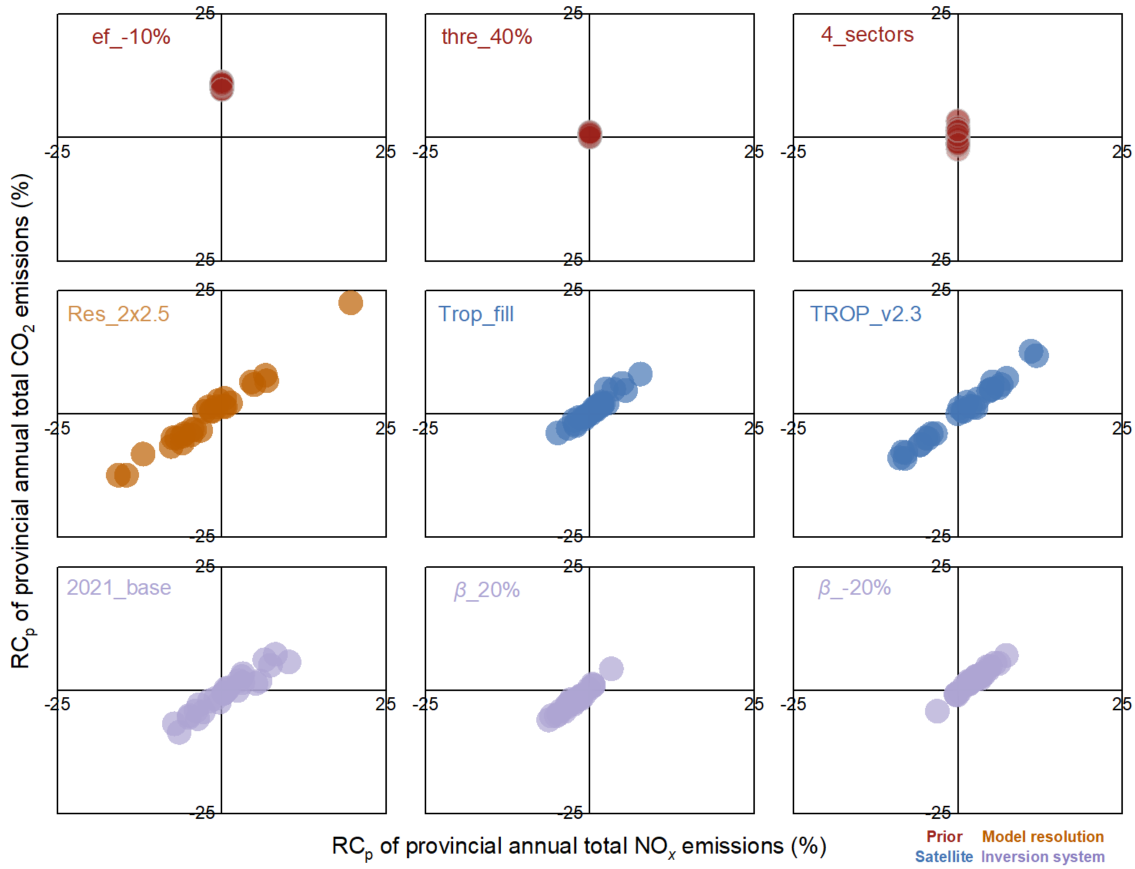

Figure S15. **Correlation between RC$_p$ in provincial annual total NO_x and CO_2 emissions.** Scatters in red, orange, blue, and purple colors show the results from the tests on prior, model resolution, satellite retrievals, and inversion system parameters, respectively.

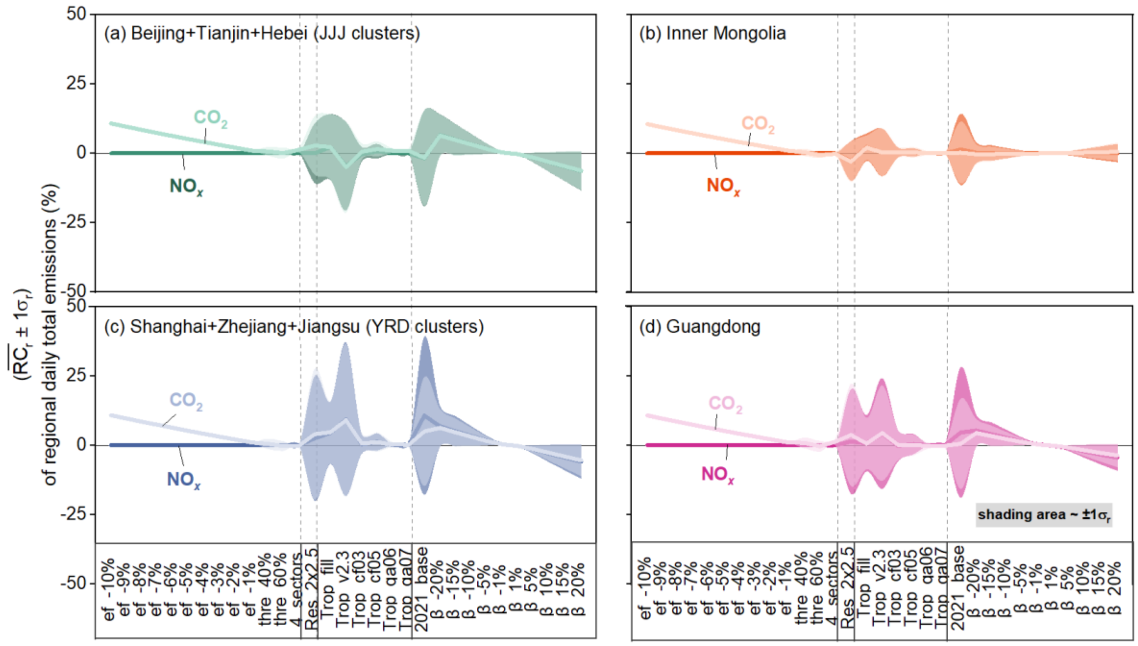

Figure S16. Response of regional total NO_x and CO_2 emissions under tests on a daily scale. (**a**), (**b**), (**c**), and (**d**) show the $\overline{RC_r} \pm 1\sigma_r$ of daily NO_x (deep color) and CO_2 (light color) emissions triggered by different tests in Jing-Jin-Ji clusters (Beijing, Tianjin, and Hebei), Inner Mongolia, Yangtze River Delta clusters (Shanghai, Zhejiang, and Jiangsu), and Guangdong.

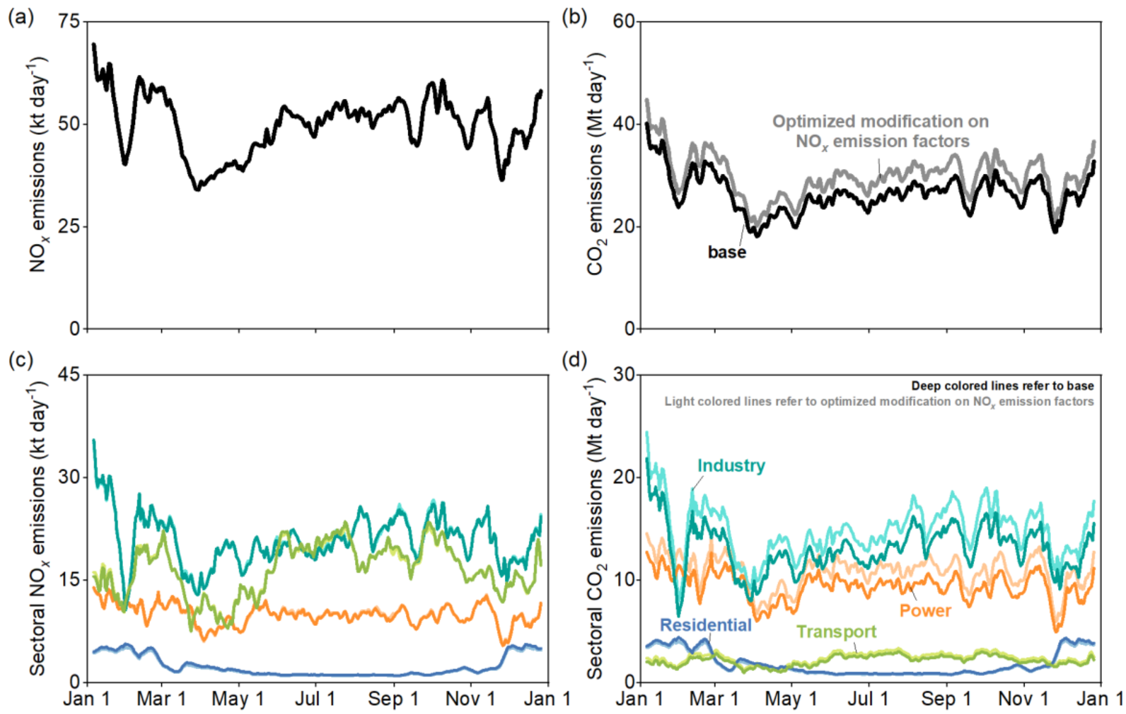

Figure S17. Comparison of daily NO_x and CO_2 emissions between base and situation with iteratively optimized modification on NO_x emission factors. (**a**) and (**c**) present the total and sectoral NO_x emissions under base (deep color) and situation with iteratively optimized modification on NO_x emission factors (light color). (**b**) and (**d**) are plotted for CO_2 as (**a**) and (**c**).

Table S1. Data sources used in the bottom-up estimates.

Steps	Corresponding MEIC sector	Adopted data	Data source
Monthly emission estimation*	Power	Thermal power generation	National Bureau of Statistics (https://data.stats.gov.cn/english/easyquery.htm?cn=C01)
	Cement	Cement production	
	Iron	Iron production	
	Other industry	Manufacturing value added	
	On-road	Road Freight turnover	
	Off-road	Construction area	
Dissolving monthly emissions into daily	Residential/ Residential-biofuel	Population-weighted heating degree day	Calculation based on the 2m temperature data from the ERA5 dataset
	Power/ Cement/ Other industry	Coal consumption	(Wu et al., 2022)
	Iron	Operating rates of electric furnace	The custeel database (https://www.custeel.com/)
	On-road/ Off-road	Baidu migration data	The Baidu database (https://qianxi.baidu.com/)

*Production index are used to differentiate January and February from the combined first two months' data in the National Bureau of Statistics.

Reference

Cheng, J., Tong, D., Liu, Y., Bo, Y., Zheng, B., Geng, G., He, K., and Zhang, Q.: Air quality and health benefits of China's current and upcoming clean air policies, Faraday Discussions, 226, 584-606, https://doi.org/10.1039/D0FD00090F, 2021.

Crippa, M., Solazzo, E., Huang, G., Guizzardi, D., Koffi, E., Muntean, M., Schieberle, C., Friedrich, R., and Janssens-Maenhout, G.: High resolution temporal profiles in the Emissions Database for Global Atmospheric Research, Scientific Data, 7, 121, 10.1038/s41597-020-0462-2, 2020.

Geng, G., Liu, Y., Liu, Y., Liu, S., Cheng, J., Yan, L., Wu, N., Hu, H., Tong, D., Zheng, B., Yin, Z., He, K., and Zhang, Q.: Efficacy of China's clean air actions to tackle $PM_{2.5}$ pollution between 2013 and 2020, Nature Geoscience, 17, 987-994, 10.1038/s41561-024-01540-z, 2024.

Li, S., Wang, S., Wu, Q., Zhang, Y., Ouyang, D., Zheng, H., Han, L., Qiu, X., Wen, Y., Liu, M., Jiang, Y., Yin, D., Liu, K., Zhao, B., Zhang, S., Wu, Y., and Hao, J.: Emission trends of air pollutants and CO_2 in China from 2005 to 2021, Earth Syst. Sci. Data, 15, 2279-2294, https://doi.org/10.5194/essd-15-2279-2023, 2023.

McDuffie, E. E., Smith, S. J., O'Rourke, P., Tibrewal, K., Venkataraman, C., Marais, E. A., Zheng, B., Crippa, M., Brauer, M., and Martin, R. V.: A global anthropogenic emission inventory of atmospheric pollutants from sector- and fuel-specific sources (1970–2017): an application of the Community Emissions Data System (CEDS), Earth Syst. Sci. Data, 12, 3413-3442, 10.5194/essd-12-3413-2020, 2020.

Wu, N., Geng, G., Qin, X., Tong, D., Zheng, Y., Lei, Y., and Zhang, Q.: Daily Emission Patterns of Coal-Fired Power Plants in China Based on Multisource Data Fusion, ACS Environmental Au, https://doi.org/10.1021/acsenvironau.2c00014, 2022.

Zheng, B., Tong, D., Li, M., Liu, F., Hong, C., Geng, G., Li, H., Li, X., Peng, L., Qi, J., Yan, L., Zhang, Y., Zhao, H., Zheng, Y., He, K., and Zhang, Q.: Trends in China's anthropogenic emissions since 2010 as the consequence of clean air actions, Atmos. Chem. Phys., 18, 14095-14111, 10.5194/acp-18-14095-2018, 2018.